Journal of Alloys and Compounds 523 (2012) 36–42

Contents lists available at SciVerse ScienceDirect

Journal of Alloys and Compounds

journal homepage: www.elsevier.com/locate/jallcom

Influence of synthesis approach on structural and magnetic properties of lithium ferrite nanoparticles

M. Abdullah Dar[a], Jyoti Shah[b], W.A. Siddiqui[a], R.K. Kotnala[b,*]

[a] Department of Applied Science & Humanities, Jamia Millia Islamia University, New Delhi 110025, India
[b] National Physical Laboratory, Dr. K.S. Krishnan Road, New Delhi 110012, India

ARTICLE INFO

Article history:
Received 29 August 2011
Received in revised form 14 January 2012
Accepted 16 January 2012
Available online 8 February 2012

Keywords:
Micro-emulsion
Super-paramagnetism
Blocking temperature
Curie temperature

ABSTRACT

Nanocrystalline $Li_{0.5}Fe_{2.5}O_4$ ferrite particles were synthesized with an average crystallite size of 12.3 nm and 5.7 nm by chemical coprecipitation and reverse microemulsion technique respectively. Zero-field cooled (ZFC) and field cooled (FC) magnetization measurements at different magnetic fields and magnetic hysteresis loops at different temperatures have been measured. The non-saturation of M–H loops with a very low coercivity and remenance at room temperature confirms the presence of superparamagnetic (SPM) nature and single-domain ferrite particles. The blocking temperature (T_B) has been found to shift towards the lower temperature region with the increase in applied magnetic field. It has been attributed to the reduction of magnetocrystalline anisotropy constant and blocking temperature dereases from 145 K to 110 K with increase in field from 50 Oe to 1000 Oe in the samples synthesized by microemulsion method. At high temperature, microemulsion synthesized nanoparticles show a maximum in magnetization versus temperature plot just below the Curie temperature (T_C) which has been attributed to the cumulative effect of the change in anisotropy with temperature and particle size growth during the measurement.

1. Introduction

The development of magnetic nano-crystalline materials is a subject of concern, both for the scientific value of understanding their unique properties and for the technological significance of enhancing the performance of existing materials. To meet the demand of high performance devices, an important step is to synthesize ferrites in nanoscale form. Below the critical size these nanocrystals exist in a single domain state, so that the domain wall resonance is avoided and the material can perform better at higher frequency [1]. The growing interest in ferrite is due to their chemical stability, biological compatibility, relative ease of preparation and a number of applications as an electronic material associated with them. These range from thermal and mechanical applications as sealants, lubricants and coolants to the challenging applications in medicine for the purpose of magnetic resonance imaging (MRI), targeted drug delivery, biosensors, gene transfer and magnetically mediated separation of bio-molecules [2–5]. One of the interesting application of ferrites is in hyperthermia treatment which is considered as a supplementary treatment to chemotherapy, radiotherapy, and surgery in cancer treatment [6]. The important structural, electrical and magnetic properties of ferrites are responsible for their applications in various fields. Nanophase ferrites have attracted much attention due to their technological importance in various fields, such as microwave devices, high speed digital tapes and disk recording, ferro-fluids, catalysis, and magnetic refrigeration systems. The physical properties of the nanomaterials are predominantly controlled by the surface effects than by the grains [7]. Nanocrystalline ferrites exhibit unusual magnetic properties such as single domain behaviour, superparamagnetism and reduced magnetization, which are not observed in the bulk material [8,9]. Superparamagnetism is a sole and important characteristic of magnetism in the nanosized magnetic materials. Understanding and controlling the superparamagnetic features of these ferrite nanoparticles is important for many applications. In nanoparticles the structure can substantially deviate from the bulk counter parts and depends upon the method of preparation and reaction conditions.

Easy methods to tailor nanoparticles of desired size, shape, composition, purity, and physical properties are extremely important for practical applications. Several synthesis methods have been developed to produce ferrite nanoparticles, that include hydrothermal [10], solvothermal [11], mechanical milling [12], sol–gel [13], bacterial synthesis [14] and so on. Most of them have been directed towards the preparation of particles, with a

* Corresponding author. Tel.: +91 11 45608599.
E-mail addresses: rkkotnala@mail.nplindia.org, rkkotnala@mail.nplindia.ernet.in (R.K. Kotnala).

0925-8388/$ – see front matter © 2012 Elsevier B.V. All rights reserved.
doi:10.1016/j.jallcom.2012.01.083

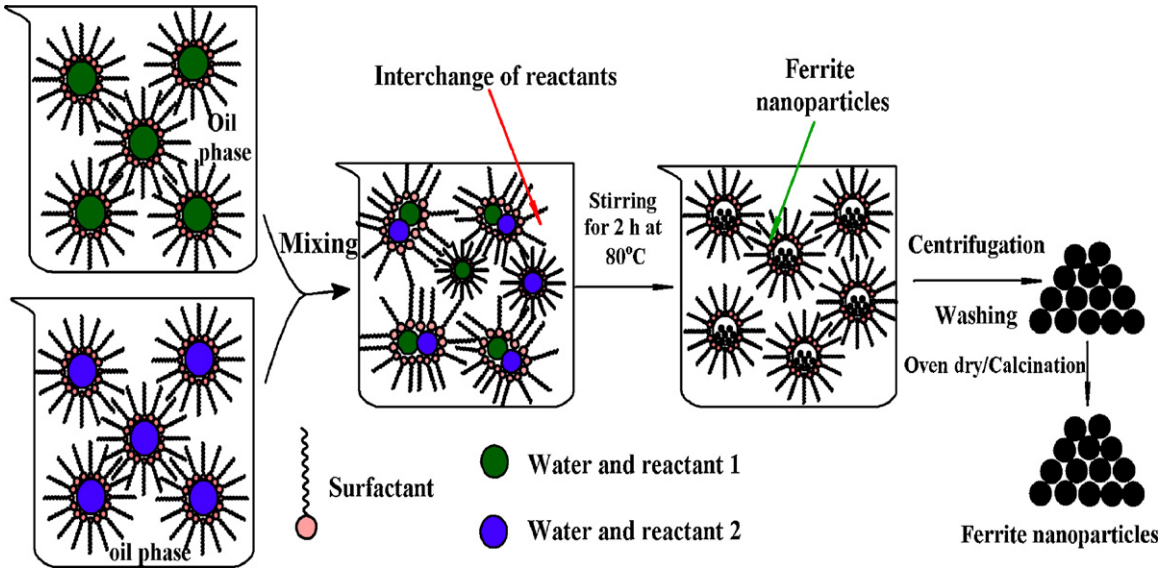

Fig. 1. Schematic representation of reverse microemulsion method for the preparation of $Li_{0.5}Fe_{2.5}O_4$ ferrite nanoparticles.

narrow size distribution in the range of few nanometers [15–17] and more recently some approaches have been experimented with the idea of achieving assemblies with suitable sizes [18–20], in particular to meet the need of biomedical applications [21,22]. However, stringent reaction conditions and complicated instrumentation in the above mentioned methods are necessary. Also the controllability of the morphology and properties of ferrite nanocrystals by these methods is limited [23]. For these reasons, it is of great importance to develop an inexpensive method to control the crystal morphology and grain size. Chemical coprecipitation, a low temperature synthesis technique is expected to control the morphology under mild reaction conditions. However, it leads to the precipitation of nanocrystals with a relatively wide range of size distribution. In order to attain very fine, monodisperse and morphologically controlled particles, a simple and efficient technique, i.e. microemulsion route has been expended in the present study to achieve the particles with desired size and magnetic properties.

Based on the surfactant-assisted strategy in aqueous media a number of methods have been developed. The surfactant plays a basic role in microemulsion, it could be taken as the ideal template for preparing nanoparticles of different shapes: spherical [24], rods [25], sheets [26], cubes [27], wires [28] and tubes [29] due to the enclosed micelles providing a space for inorganic crystal growth. Some methods are reported to give rise to the formation of either single ferrite nanoparticles [30] or to the formation of various superstructures from primary nanoparticles [15–17]. However, nothing has been reported about the conditions that can be used to produce either individual nanoparticles or their assemblies. Some workers have reported on the synthesis and fabrication of monodisperse multicomponent ferrite nanocrystals via reverse microemulsion [31,32] method, but to the best of our knowledge none of these has been devoted to the synthesis of $Li_{0.5}Fe_{2.5}O_4$ ferrite nanocrystals by reverse microemulsion method.

In the present studies we have reported the synthesis of $Li_{0.5}Fe_{2.5}O_4$ ferrite nanocrystals by chemical coprecipitation method and reverse microemulsion method. The structural and morphological analyses have been carried out by X-ray diffraction and transmission electron microscopy. The magnetic properties of the synthesized nanocrystals have been investigated by using vibrating sample magnetometer at different temperatures. Zero-field cooled (ZFC) and field cooled (FC) magnetization measurements at different fields and magnetic hysteresis loops at different temperatures have been measured. Also a comparative study of chemical coprecipitation with reverse microemulsion process has been carried out.

2. Experimental

2.1. Synthesis of $Li_{0.5}Fe_{2.5}O_4$ ferrite nanocrystals by reverse microemulsion method

All the chemicals used in this work were of analytical grade. The preparation procedure steps of $Li_{0.5}Fe_{2.5}O_4$ ferrite nanoparticles by the reverse microemulsion technique are shown in Fig. 1, with cyclohexane as oil, cetyl-tri-methyl-ammonium bromide (CTAB) as surfactant, isoamylalcohol as the co-surfactant phase. Microemulsions were prepared by adding to 10.20 g of CTAB, 12.81 ml of isoamylalcohol and 30.48 ml of cyclohexane with 5.5 wt% of an aqueous solution of the reactants, corresponding to the desired value of water/[CTAB] ratio being equal to 10.12. The emulsions were sonicated until clear solutions were formed. In order to synthesize $Li_{0.5}Fe_{2.5}O_4$ ferrite, two microemulsions were prepared: one containing the metal salts prepared by mixing stoichiometric amounts of 0.125 M $Fe(NO_3)_3{\cdot}9H_2O$ and 0.025 $Li(NO_3)_2{\cdot}6H_2O$. Second reverse micro-emulsion solution was prepared with 0.1 M aqueous solution of NaOH as water phase under similar conditions. The solutions were mixed together quickly with vigorous stirring at constant temperature (80 °C) and pH of the resulting solution was maintained at 9. The resulting solution was continuously stirred for another 2 h in order to complete the reaction. An equal volume of acetone and isopropanol was added to the resulting solution and was centrifuged to separate the solid product. The product obtained was washed several times with water and acetone followed by drying in an air oven at 100 °C for 36 h.

2.2. Synthesis of $Li_{0.5}Fe_{2.5}O_4$ ferrite nanocrystals by chemical coprecipitation method

In a typical procedure, nanocrystals of $Li_{0.5}Fe_{2.5}O_4$ ferrite were prepared by chemical coprecipitation of Fe^{3+} and Li^{1+} in an alkaline medium at constant pH of 9. The stock solutions of all the precursors were prepared with same concentration as followed in reverse microemulsion method. The stoichiometric amount of $Fe(NO_3)_3{\cdot}9H_2O$ and $Li(NO_3)_2{\cdot}6H_2O$ were mixed. Then this mixture was poured into 0.1 M NaOH solution under stirring at constant temperature of 80 °C. The resulting mixture was continuously stirred for 2 h at same temperature and pH. The resulting precipitate obtained was filtered off and washed several times with methanol and double distilled water followed by drying in an air oven at 100 °C for 36 h.

2.3. Theory

Inducing precipitation of a compound, however does not guarantee that the product will be nano-particulate, regular shaped and monodispersed. The processes of nucleation and growth govern the particle size and morphology of products in precipitation reactions. When precipitation begins, numerous small crystallites initially form (nucleation) but they tend to quickly aggregate together to form larger, thermodynamically more stable particles (growth). To produce nanoparticles, the nucleation process must be relatively fast in comparison to the growth one. The formation of particles with a narrow size distribution requires that the nuclei of all species should form simultaneously and inhibiting subsequent nucleation of smaller

particles. The thermodynamics that favours the maximization of the surface/volume ratio, while the agglomeration of small particles precipitated from solutions is practically inevitable in the absence of a stabilizer.

The amphiphilic nature of the surfactants makes them miscible in both water and hydrocarbons but when the surfactant is mixed with a hydrocarbon resulting in mixture which is low in viscosity, isotropic, and very stable. The surfactant molecules through ion–dipole interactions with the polar co-surfactant forms spherical aggregates in which the polar ends of the surfactant molecules orient towards the center. The co-surfactant acts as an electronegative "spacer" that diminishes repulsions between the positively charged surfactant heads [33]. The addition of water to the system will cause the aggregates to expand from the center as the water molecules again as a result of ion–dipole and dipole–dipole interactions situate at the center of the sphere. The orientation of molecules in microemulsion minimizes the interfacial tension between aggregates due to which microemulsions are thermodynamically stable in comparison to macroemulsions. It is important to recognize that these systems are dynamic, i.e. micelles frequently collide via random Brownian motion and coalesce to form dimers which may exchange contents in their aqueous cores and also break apart again resulting in the equilibrium distribution of all contents [34]. Inorganic reagents that were encapsulated inside the micelles will become mixed. This exchange process is basis for nanoparticle synthesis inside reversed micellar templates allowing different reactants solubilized in separate micellar solutions to react upon mixing. Micelles in these systems can be described as nanoreactors, providing a suitable environment for controlled nucleation and growth. In addition, at the latter stages of growth, steric stabilization provided by the surfactant layer prevents the nanoparticles from aggregation [35]. Since the size of the water pools in reverse micelles can be controlled by adjusting water/surfactant ratio (ω_0) and the Brownian motion of the particles. It allows the distribution of reactants and reactions can be performed inside the micellar cores besides products will have nearly uniform size and shape. Solvated ions tend to affect both the stability of reverse micelles and the phase equilibrium. In particular, solvated ions in reverse micelles formed from ionic surfactants causes a contraction of micelle radius due to its interactions with the charged surfactant heads and allows micelles to be more spherical. Moreover, the influence of solvated ions on micelle radius tends to increase with increasing concentration and charge.

Experiments focusing on the interfacial water of reverse micelles have confirmed that the water molecules in close proximity to the surfactant are greatly influenced by dipole–dipole and ion–dipole interactions with the ionic surfactants and polar co-surfactants are largely immobilized. The water at the reverse micelle core is affected to a lesser extent but the immobilization of the interfacial water reduces the effective radius of the core water pool. The presence of the surfactant molecules in the reverse micelle to some extent acts as capping agents and hence prevents flocculation of the particles.

2.4. Characterization

X-ray diffraction (XRD) analysis for determining crystallinity and phase purity of samples was carried out using Rigaku Miniflex (step size = 0.02) with CuKα radiation of wavelength λ = 1.5406 Å. The particle size, morphology and SAED patterns of both the ferrite samples were determined using high-resolution transmission electron microscopy (JEM 200CX model). Finely ground samples were dispersed in methanol followed by ultrasonication were mounted on carbon-coated copper grids. The variation of magnetization as a function of magnetic field, up to a maximum field of 5 kOe at different temperatures (80–1000 K) and at different applied magnetic fields, was measured by vibrating sample magnetometer (Lakeshore, 7304). The zero field cooled magnetization was carried out by cooling the sample in a zero magnetic field from 300 K to 80 K followed by magnetization measurement while increasing the temperature from 80 K to 300 K under the influence of applied magnetic field of 50 Oe. Field cooled measurements were performed in the same manner except the cooling of the samples was done in the same field of 50 Oe. ZFC–FC measurements were performed at two different applied magnetic fields 50 Oe and 1000 Oe in order to study the effect of applied field on the blocking temperature (T_B).

3. Results and discussion

Fig. 2 shows the X-ray diffraction patterns of nanocrystalline $Li_{0.5}Fe_{2.5}O_4$ ferrite samples 'a' and 'b' obtained from chemical coprecipitation and reverse microemulsion technique respectively. The sharp peaks from diffraction pattern show the crystalline nature of the samples. All the diffraction peaks could be ascribed to the reflections of (2 2 0), (3 1 1), (4 0 0), (4 2 2), (5 1 1), and (4 4 0) planes which could be indexed to a face-centred cubic $Li_{0.5}Fe_{2.5}O_4$ ferrite phase. It confirms that ferrite spinel phase is formed without the presence of any other impurity phase. The reflections are comparatively broader, revealing that as-prepared nanocrystals are small in size. According to the Debye–Scherrer equation [13], the average crystallite size was determined from the half-width of

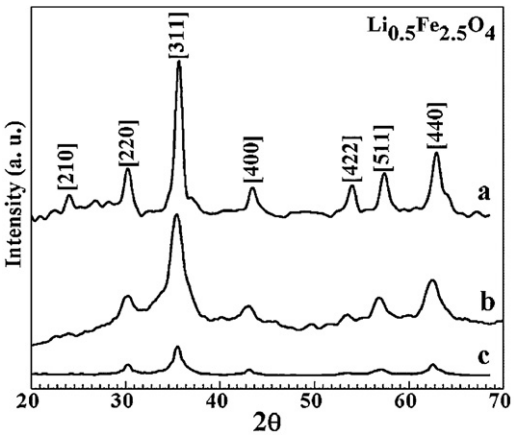

Fig. 2. XRD pattern of $Li_{0.5}Fe_{2.5}O_4$ ferrite nanocrystals obtained from (a) chemical co-precipitation method (b) reverse microemulsion method for 36 h and (c) reverse microemulsion method for 6 h.

the most intense peak (3 1 1) and found to be 12.3 nm and 5.7 nm for sample 'a' and 'b' respectively, which are in close agreement with the TEM results. The difference in crystallite size was probably due to the different preparation conditions followed in this work. It gave rise to different rates of nucleation, growth, coarsening, and agglomeration processes and hence favouring the variation in crystallite size. The X-ray diffraction pattern of $Li_{0.5}Fe_{2.5}O_4$ ferrite nanocrystals obtained from the chemical coprecipitation method exhibits the more intense peaks, indicating their higher crystallinity as shown in Fig. 2. From figure it is also apparent that the XRD pattern of sample 'b' loses some characteristic peaks of lithium ferrite and shows some peak shift compared to the XRD pattern of sample 'a'. This is attributed to the fact that in microemulsion synthesized samples the crystals are of small size in comparison to the coprecipitation synthesized samples due to internal strain induced in the lattice. This effect causes the lattice plane spacing to change and the diffraction peaks are observed to show a shift in the diffraction pattern. The appearance of diffraction peaks in a sample depends upon the distribution of inter-atomic distances within the scattering volume. These inter-atomic distances are reduced by the decrease in the crystallite size and hence resulted in the disappearance of some low intensity diffraction peaks. Fig. 2(c) represents the XRD pattern of microemulsion synthesized sample heated at 100 °C for 6 h. From this figure it is clear that pure phase $Li_{0.5}Fe_{2.5}O_4$ nanocrystals are even formed at 6 h heating, but the nanocrystals formed are of low crystallinity as shown in Fig. 2(c). In order to increase the crystallinity, we performed long duration heating (100 °C for 36 h) of our samples [36]. The lattice constant for $Li_{0.5}Fe_{2.5}O_4$ ferrite nanocrystals prepared by chemical coprecipitation and reverse microemulsion were found to be 8.34 Å and 8.36 Å respectively.

Fig. 3(a) and (b) shows the transmission electron microscopy (TEM) images of $Li_{0.5}Fe_{2.5}O_4$ nanoparticles synthesized by chemical coprecipitation and reverse microemulsion technique respectively. The particle size distribution and their selected area electron diffraction (SAED) patterns are included as insets in Fig. 3(a) and (b). These SAED patterns correspond to various diffraction patterns, confirming of a spinel phase presence consistent with the results obtained from powder XRD analysis. The digitized images were imported into the program, Image J and the size of particles with respect to mean particle diameter was determined. To estimate the average particle size of each sample, the average diameter of about 80 nanoparticles were measured from different micrographs. Fig. 3(a) confirms that the particles obtained by chemical coprecipitation method are irregular shaped and the average particle size obtained from TEM is bigger than that observed from X-ray

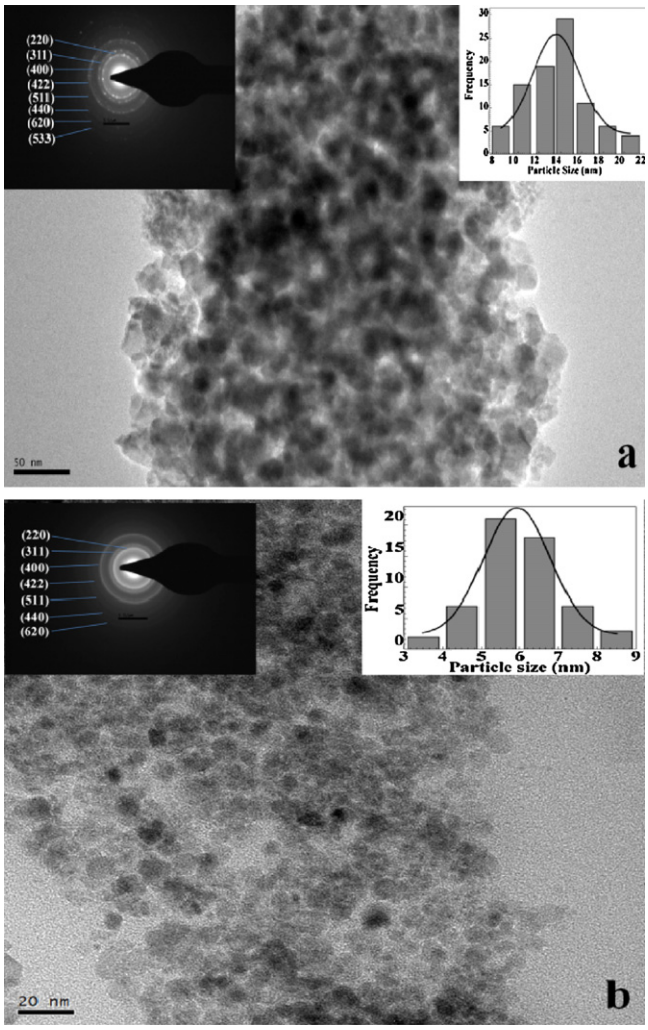

Fig. 3. TEM images of nanocrystals obtained from (a) chemical co-precipitation and (b) reverse microemulsion method. The inset in figure (a) and (b) shows selected area electron diffraction pattern and histogram of the particle size distribution.

line broadening technique. This may be due to the highly agglomerated particles of Li ferrite as it is evident from Fig. 3(a). Reverse microemulsion process has resulted into the slightly agglomerated, nearly monodisperse and spherical particle size distribution with reduced average diameter in the range of 5–6 nm, compared to the coprecipitated synthesized samples as shown in Fig. 3(b). The average crystallite size D_{XRD}, D_{TEM} and the lattice constant 'a_o' of $Li_{0.5}Fe_{2.5}O_4$ nanocrystals are summarized in Table 1.

Zero-field cooled and field cooled magnetization measurements under different fields and magnetic hysteresis loops at different temperatures have been performed for as-synthesized samples of $Li_{0.5}Fe_{2.5}O_4$ ferrite. The ZFC curve was generated by cooling the sample in zero field, subsequently applying the magnetic field at low temperature and simeltaneously measuring the magnetization while increasing the temperature. It exhibits a maximum at a temperature commonly referred as blocking temperature (T_B) of

Table 1
Various structural parameters of as-synthesized $Li_{0.5}Fe_{2.5}O_4$ nano-crystals.

Composition	Lattice parameter (Å)	Crystallite size (nm)	
$Li_{0.5}Fe_{2.5}O_4$	a_o	D_{TEM}	D_{XRD}
Co-precipitation	8.34	13–15	12.3
Micro-emulsion	8.36	5–6	5.7

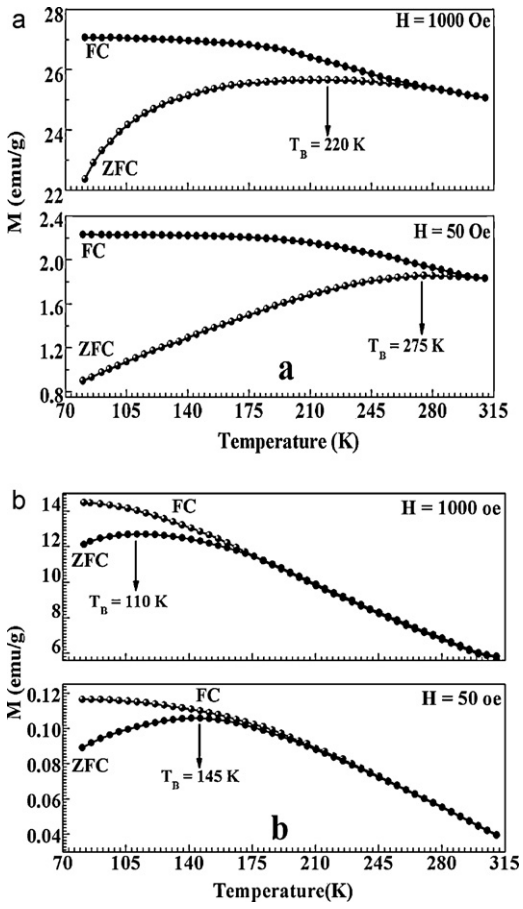

Fig. 4. ZFC–FC curves of $Li_{0.5}Fe_{2.5}O_4$ ferrite nanocrystals obtained from (a) chemical co-precipitation and (b) reverse microemulsion method recorded at 50 Oe and 1000 Oe for $Li_{0.5}Fe_{2.5}O_4$ nanocrystals.

the sample. T_B is known as the temperature at which the magnetic anisotropy energy barrier of a magnetic single domain particle is overcomed by thermal activation energy leading to the variation of the magnetization direction. At temperatures above T_B, the thermal energy, characterized by k_BT is larger than the magnetic energy barrier and thus the materials become superparamagnetic (SPM) following the Curie–Weiss law. ZFC and FC magnetization curves bifurcated at the blocking temperature (T_B) while ZFC magnetization shows a peak at a temperature T_{SEP}, which is lower than the blocking temperature. In a nanoparticle system, the temperature T_B can be regarded as the highest temperature at which the ZFC and FC magnetizations bifurcated corresponding to the larger particles in the system, and the ZFC magnetization decreases below the temperature T_{SEP} due to the smaller group of particles in the system. Thus the different values of T_B and T_{SEP} are due to the particle size distribution and dipole–dipole interaction of the SPM particles, resulting in a distribution of the blocking temperature in the samples rather than the exact value, which is also in agreement with the findings of TEM analysis [37]. For this type of distribution some fraction of particles is interacting even at room temperature, which is evident from the non-zero value of coercivity in the magnetic measurements at this temperature [37]. The fact that the FC curve was nearly flat below T_B as compared with the monotonically increasing behaviour characteristic of non-interacting systems which indicates the existence of strong interactions among the nanoparticles synthesized by coprecipitation method in contrast with our sample results synthesized by reverse microemulsion method [38]. Fig. 4(a) and (b) shows the ZFC–FC curves recorded at different applied fields for $Li_{0.5}Fe_{2.5}O_4$ nanocrystals synthesized via chemical

coprecipitation and reverse microemulsion method respectively. From the curves it is clear that the blocking temperature T_B shifts to lower temperature with increase in applied field and it is attributed to the reduction of magnetocrystalline anisotroppy constant. From these plots, the blocking temperature (T_B) for both the samples synthesized by chemical coprecipitation and microemulsion method are 275 K and 145 K at 50 Oe and 220 K and 110 K at 1000 Oe respectively. When a magnetic field is applied to a magnetic material, the domain walls rotate in such a way that its multidomain structure changes more towards a single-domain structure with increase in the field. In addition to the extrinsic factors such as defects and lattice strains another very important factor that plays a crucial role in determining the domain wall motion is the magnetocrystalline anisotropy.

The magnetocrystalline anisotropy of a single-domain particle is given by $E_A = KV\sin^2\theta$, where K is the magnetocrystalline anisotropy constant, V is the volume of the nanoparticle and θ is the angle between the direction of magnetization and the easy axis of the nanoparticle. KV is the anisotropy energy barrier for the reversal of magnetic moment [39]. The cation distribution in a particular ferrite also plays a dominant role in the resultant blocking temperature.

The reversal or switching time called the Neel relaxation time is given by the relation (1):

$$\tau = \tau_o exp\left(\frac{E_A}{k_B T_B}\right) \quad (1)$$

or

$$E_A = \ln\left(\frac{\tau}{\tau_o}\right) k_B T_B \quad (2)$$

where τ is the super-paramagnetic relaxation time (30 s), τ_o is a relaxation time constant ($\sim 10^{-10}$ s) and T_B is the blocking temperature. The anisotropy is larger for nanocrystalline material than the bulk one and it increases with the decrease in particle size as well as it decreases with the increase in applied magnetic field. Assuming the particles to be spherical, the magnetocrystalline anisotropy constant K values obtained for samples 'a' and 'b' are 8.7×10^5 erg/cm^3 and 47.8×10^5 erg/cm^3 at 50 Oe and 6.8×10^5 erg/cm^3 and 36.2×10^5 erg/cm^3 at 1000 Oe respectively. These values are substantially higher than the bulk ferrites.

Variation of magnetization with the applied field at a temperature of 310 K are depicted in Fig. 5(a) and (b) for both the ferrite samples prepared by coprecipitation and microemulsiom method respectively. The typical characteristics of SPM behaviour like very low coercivity and remenance, and the non-attainment of saturation even at the magnetic field of 5 kOe are observed. The non-saturation of M–H loop, and very low coercivity and remenance values (Fig. 5) at 310 K is indicative of the presence of SPM and single-domain particles for both the materials. Below T_B, the nanoparticles of these ferrites indicated remanence and coercivity exhibited in hysteresis plot at 80 K is shown in Fig. 5(a) and (b) for both the samples prepared by coprecipitation and microemulsiom method respectively. At this temperature the particles do not have adequate thermal energy to attain complete thermal equilibrium with the applied field during the measurement time and hence, hysteresis appears. From Fig. 5(a) and (b), it may be noted that the remanent magnetization and coercivity values for sample 'a' at 80 K are 7.8 emu/g and 262 Oe respectively, and for the sample 'b' are 1.1 emu/g and 44 Oe respectively. The hysteritic behaviour and the ZFC–FC separation of both the samples suggests the high field irreversibility below the blocking temperature. The magnetization of both the samples is not strictly saturated even at 80 K with applied maximum field of 5 kOe. It is clear from Fig. 5 that the slope of the magnetization curve increases at high field once temperature is decreased. The increase in the slope may be attributed to

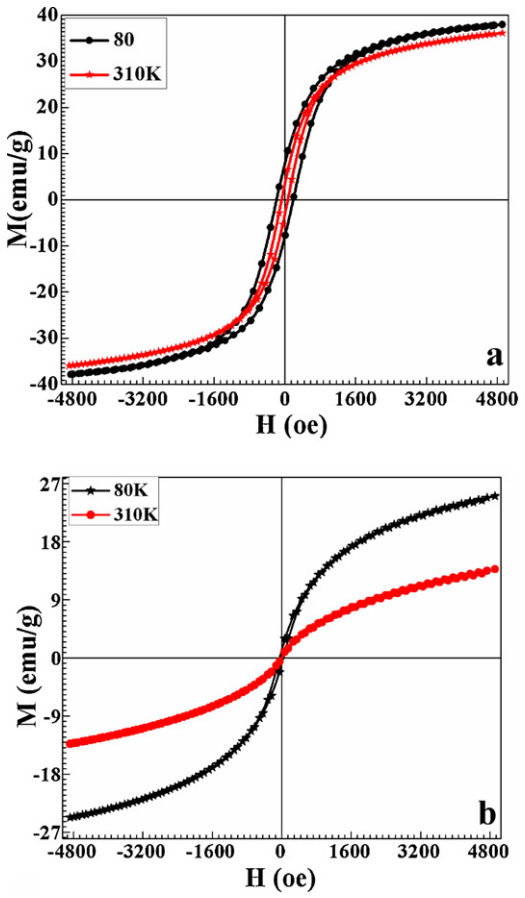

Fig. 5. The M–H curves of $Li_{0.5}Fe_{2.5}O_4$ ferrite nanocrystals obtained from (a) chemical co-precipitation and (b) reverse microemulsion method measured with an applied field of 5 kOe at 80 K and 310 K.

the increase in magnetic anisotropy which is related to the surface magnetism of the nanoparticles [37]. The lower value of highest magnetization (36 emu/g and 13.7 emu/g for 'a' and 'b' samples) of nanocrystalline ferrites compared to the multidomain bulk values of 70 emu/g at 5000 Oe is attributed to the increased cation disorder and surface effects in nanocrystalline ferrites. This can be explained in terms of the core–shell morphology of the nanoparticles consisting of ferrimagnetically aligned core spins and a spin-canted like surface layer. The spin disorder from the surface of the nanoparticles may essentially modulate the magnetic properties of these materials especially when the surface/volume ratio is large enough [40]. Up to a particular magnetic field, the core magnetic moments align with the applied magnetic field. At some stage, the resource of the 'core mode' of the magnetization response is exhausted and the 'core magnetization' of the system is saturated in a usual Langevin-like way. Beyond this stage, any increase in the magnetic field on the particles has an effect only on the surface layer of the particles and thus the increase in the magnetization of particles slows down. This specific state of the surface results in the absence of magnetic saturation and keeps the hysteresis loops unclosed even in very strong fields [41]. The surface layer magnetic moment anomalies may be due to the broken exchange bonds, high anisotropy layer on the surface or loss of the long-range order in the surface layer. An increase in the magnetocrystalline anisotropy can also result from the inter-particle interactions, which are more intense in case of ferrites because of the super-exchange interactions. The presence of any defect on the surface leads to the weakening of these interactions inducing a large surface spin disorder [42]. The variation of the coercivity with temperature in $Li_{0.5}Fe_{2.5}O_4$ ferrite samples

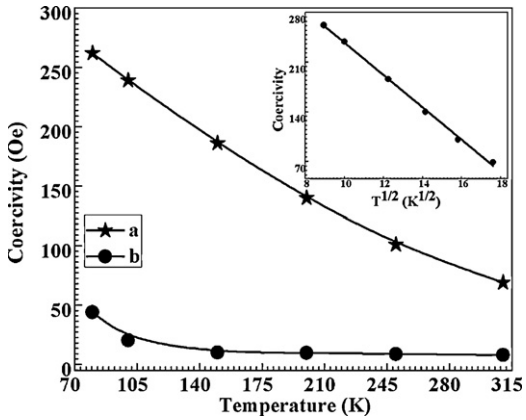

Fig. 6. Variation of coercivity with temperature of $Li_{0.5}Fe_{2.5}O_4$ ferrite nanocrystals obtained from (a) chemical co-precipitation and (b) reverse microemulsion method. The inset shows that the sample b shows linear variation with $\sqrt{T}$.

prepared by coprecipitation and reverse microemulsion method are depicted in Fig. 6. It is evident from this figure that the coercivity is strongly dependent on temperature. It may be due to the fact that for a particle to reverse its spin, it should have enough thermal energy to overcome the energy barrier $\Delta E = KV$. At higher temperature the particles have higher thermal energy, and hence they require smaller field to reverse the magnetization. The coercivity relation of the magnetic nanoparticles with Curie temperature is given by Eq. (3) [43]:

$$H_C = \frac{2K}{M_S}\left[1 - \left(\frac{25k_BT}{kV}\right)^{1/2}\right] \quad (3)$$

The coercivity field of sample 'a' has been found to decay linearly with the square root of temperature as shown in the inset of Fig. 6. However for sample 'b', a deviation from the linearity is observed. This means that any observed variation of H_C with temperature is not only due to the thermal effects but to other causes, such as the variation of K and M_S with temperature. The occurrence of finite coercivity at room temperature is attributed to the presence of larger particles within the distribution.

The magnetic measurements of $Li_{0.5}Fe_{2.5}O_4$ ferrite were also performed above the room temperature up to 1000 K in order to determine the effect of synthesis process on the Curie temperature (T_C). The Curie temperature of $Li_{0.5}Fe_{2.5}O_4$ ferrite nanocrystals obtained from coprecipitaion and reverse microemulsion method was found to be 890 K and 840 K respectively as shown in Fig. 7(a) and (b). From these graphs it is clear that T_C is less for the sample 'b' synthesized by microemulsion method. This could be due to the effect of frustrated super-exchange interactions developed by the cation disorder and spin canting on the surface region of nanoparticles. The magnetization is observed to show a continuous decrease with increasing temperature and reaches a minimum value at the Curie temperature for sample 'a' as it is shown in Fig. 7(a). This may be due to ferromagnetic character of the samples prepared by coprecipitation method as is evident from M–H curve shown in Fig. 5(a). The decrease in magnetization is mainly attributed to the thermal randomization of the magnetic moments. For the smaller particles of sample 'b', the magnetization decreases to a minimum value as the temperature is increased then increases to a maximum and is followed by a drop down to zero at T_C as depicted in Fig. 7(b). A maximum in the magnetization curve just below the T_C in the presence of a small magnetic field is commonly referred as the Hopkinson effect. The maximum in the magnetization just below the T_C is essentially a competitive effect between the applied magnetic field (H) and the magnetocrystalline anisotropy field (H_a). The magnetization has been found to decrease intially for sample

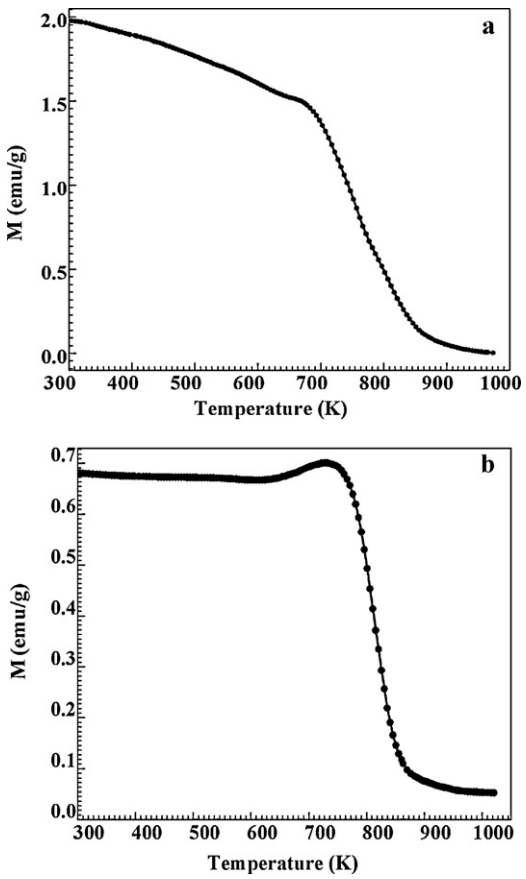

Fig. 7. The magnetization versus temperature graphs of $Li_{0.5}Fe_{2.5}O_4$ ferrite nanocrystals obtained from (a) chemical coprecipitation and (b) reverse microemulsion method measured with an applied field of 50 Oe.

'b' which is mainly attributed to the thermal randomization of the magnetic moments. With increasing temperature unstable superparamagnetic particles become stable single domain particles. This magnetic phase transition occurs simultaneously with the fall of anisotropy field (H_a) to a negligible value. Therefore the magnetic moment vectors of these nanoparticles with negligible anisotropy tend to align towards the direction of applied field (H) resulting in the steep rise of magnetization just below the T_C and on further increasing the temperature results in the demagnetization of magnetic moments at the Curie temperature [44]. In Fig. 7(b) initial slow decrease in magnetization value with temperature confirms superparamagnetic nature of the nanoparticles (5.7 nm) compared to Fig. 7(a) plot. Fig. 5(b) explicitly shows M–H plot as superparamagnetic nature of sample prepared by reverse microemulsion method.

4. Conclusions

A novel and facile route of reverse microemulsion method has been demonstrated here for the synthesis of nanocrystalline $Li_{0.5}Fe_{2.5}O_4$ ferrite. The synthesis procedure developed here offers several advantageous features for the synthesis of magnetic nanocrystals over other conventional methods. Utilization of this method has resulted into the formation of much finer, nearly monodisperse and spherical particles compared to the irregular shaped particles obtained by the coprecipitation method with an average diameter of 5.7 nm. The presence of the surfactant molecules in the micelles, which to some extent act as capping agents, may serve to prevent agglomeration of the particles. The highest magnetization value of $Li_{0.5}Fe_{2.5}O_4$ ferrite nanocrystals

prepared by reverse microemulsion technique (13.7 emu/g) has been found less than those particles prepared by chemical coprecipitation (36 emu/g) and their bulk counter parts (70 emu/g) at the same applied magnetic field (5 kOe). It has been explained in terms of the core–shell morphology of the nanoparticles consisting of ferrimagnetically aligned core spins and a spin-canted like surface layer. The coercivity has been observed to decrease with temperature, however a deviation from the linearity is observed in reverse microemulsion synthesized sample. This means that any observed variation of coercivity is not only due to the thermal effects, but to other effects such as the variation of K and M_S with temperature. The anisotropy has been observed to increase substantially with the decrease in particle size as well as decreases with the increase of applied magnetic field. The reverse microemulsion route has shown a significant effect on blocking as well as on Curie temperature of the ferrite nanocrystals. The Curie temperature for the sample synthesized by microemulsion method was found low as compared to the coprecipitated sample (840 K and 890 K respectively). It could be explained by the effect of frustrated super-exchange interactions due to the cation disorder and spin canting in the surface region of nanoparticles. At high temperature magnetization, microemulsion synthesized nanoparticles were observed to show a maximum immediately below the Curie temperature and are explained in terms of the collective effect of the temperature variation of the anisotropy and particle size growth during the measurements.

Acknowledgements

The authors are grateful to Director, National Physical Laboratory; New Delhi for providing constant encouragement and motivation to carry out this work. To carry out this work financial assistance from University Grants Commission is highly acknowledged by M. Abdullah Dar through grant no. F1-17.1/2011/MANF-MUS-JAM-638.

References

[1] B.P. Rao, A.M. Kumar, K.H. Rao, Y.L.N. Murthy, O.F. Caltun, I. Dumitru, L. Spinu, J. Optoelectron. Adv. Mater. 8 (2006) 1703–1705.
[2] A. Nacev, C. Beni, O. Bruno, B. Shapiro, J. Magn. Magn. Mater. 323 (2011) 651–668.
[3] L. Wang, J. Ren, Y. Wang, X. Liu, Y. Wang, J. Alloys Compd. 490 (2010) 656–660.
[4] C.L. Dennis, A.J. Jackson, J.A. Borchers, P.J. Hoopes, R. Strawbridge, A.R. Foreman, Nanotechnology 20 (2009) 3951031–3951037.
[5] M. Hashimoto, Y. Hisano, J. Neurosci. Methods 194 (2011) 316–320.
[6] J. Chandradass, K.H. Kim, J. Alloys Compd. 509 (2011) L59–L62.
[7] S.T. Alone, S.E. Shirsath, R.H. Kadam, K.M. Jadhav, J. Alloys Compd. 509 (2011) 5055–5060.
[8] A. Pradeep, P. Priyadharsini, G. Chandrasekaran, J. Alloys Compd. 509 (2011) 3917–3923.
[9] Q. Chen, Z.J. Zhang, Appl. Phys. Lett. 73 (1998) 3156–3158.
[10] V. Cabuil, V. Dupuis, D. Talbot, S. Neveu, J. Magn. Magn. Mater. 323 (2011) 1238–1241.
[11] M. Jean, V. Nachbaur, J.M.L. Breton, J. Alloys Compd. 513 (2012) 425–429.
[12] T.F. Marinca, I. Chicinaş, O. Isnard, V. Pop, F. Popa, J. Alloys Compd. 509 (2011) 7931–7936.
[13] M. Abdullah Dar, K.M. Batoo, V. Verma, W.A. Siddiqui, R.K. Kotnala, J. Alloys Compd. 493 (2010) 553.
[14] L.W. Yeary, J.W. Moon, C.J. Rawn, L.J. Love, A.J. Rondinone, J.R. Thompson, B.C. Chakoumakos, T.J. Phelps, J. Magn. Magn. Mater. 323 (2011) 3043–3048.
[15] R. Abu-Much, A. Gedanken, J. Phys. Chem. C 112 (2008) 35.
[16] T. Hyeon, Y. Chung, J. Park, S.S. Lee, Y.W. Kim, B.H. Park, J. Phys. Chem. B 106 (2002) 6831.
[17] F. Vereda, J. De Vicente, R. Hidalgo-Alvarez, Langmuir 23 (2007) 3581.
[18] L.E. Euliss, S.G. Grancharov, S.O. Brien, T.J. Deming, G.D. Stucky, C.B. Murray, G.A. Held, Nano Lett. 3 (2003) 1489.
[19] Y. Zhu, W. Zhao, H. Chen, J. Shi, J. Phys. Chem. C 111 (2007) 5281.
[20] B. Jia, L. Gao, J. Phys. Chem. C 112 (2008) 666.
[21] Q.A. Pankhurst, J. Jones, S.K. Connolly, J. Dobson, J. Phys. D: Appl. Phys. 36 (2003) 167.
[22] H. Deng, X. Li, Q. Peng, X. Wang, J. Chen, Y. Li, Angew. Chem. Int. Ed. Engl. 44 (2005) 2782.
[23] S. Kumar, V. Singh, S. Aggarwal, U.K. Mandal, R.K. Kotnala, J. Phys. Chem. C 114 (2010) 6272–6280.
[24] J. Wang, F. Ren, R. Yi, A. Yan, G. Qiu, X. Liu, J. Alloys Compd. 479 (2009) 791–796.
[25] D.E. Zhang, X.J. Zhang, X.M. Ni, H.G. Zheng, D.D. Yang, J. Magn. Magn. Mater. 292 (2005) 79–82.
[26] J.L. Gunjakar, A.M. More, K.V. Gurav, C.D. Lokhande, Appl. Surf. Sci. 254 (2008) 5844–5848.
[27] X.F. Chu, D.L. Jiang, C.M. Zheng, Sens. Actuators B 123 (2007) 793–797.
[28] V. Musat, O. Potecasu, R. Belea, P. Alexandru, Mater. Sci. Eng. B 167 (2010) 85–90.
[29] M. Harada, M. Adachi, Adv. Mater. 12 (2000) 839.
[30] N. Feltin, M.P. Pileni, Langmuir 13 (1997) 3927.
[31] M.N. Ashiq, M.F. Ehsan, M.J. Iqbal, I.H. Gul, J. Alloys Compd. 509 (2011) 5119–5126.
[32] H.F. Lu, R.Y. Hong, H.Z. Li, J. Alloys Compd. 509 (2011) 10127–10131.
[33] J.H. Schulman, D.P.J. Riley, Colloid Sci. 3 (1948) 383.
[34] J.H.R. Clarke, J.D. Nicholson, K.N.J. Regan, Chem. Soc. Faraday Trans. 81 (1985) 1173.
[35] M.A. Lopez-Quintela, C. Tojo, M.C. Blanco, L. Garcia Rio, J.R. Leis, Curr. Opin. Colloid Interface Sci. 9 (2004) 264–278.
[36] G. Vaidyanathan, R. Arulmurugan, S.D. Likhite, M.R. Anantharaman, Milind Vaidya, S. Sendhilnathan, N.D. Senthilram, Indian J. Eng. Mater. Sci. 11 (2004) 289–294.
[37] S. Modak, S. Karan, S.K. Roy, P.K. Chakrabarti, J. Appl. Phys. 108 (2010) 0939121–0939129.
[38] T. Bitoh, K. Ohba, M. Takamatsu, T. Shirane, S. Hikazawa, J. Phys. Soc. Jpn. 64 (1995) 1305.
[39] V. Verma, M. Abdullah Dar, V. Pandey, A. Singh, S. Annapoorni, R.K. Kotnala, Mater. Chem. Phys. 122 (2010) 133–137.
[40] N.M. Deraz, J. Alloys Compd. 501 (2010) 317–325.
[41] S. Thakur, S.C. Katyal, M. Singh, J. Magn. Magn. Mater. 321 (2009) 1–7.
[42] J. Chandradass, M. Balasubramanian, K.H. Kim, J. Alloys Compd. 506 (2010) 395–399.
[43] M. George, A.M. John, S.S. Nair, P.A. Joy, M.R. Anantharaman, J. Magn. Magn. Mater. 302 (2006) 190–195.
[44] S. Verma, P.A. Joy, J. Appl. Phys. 98 (2005) 124312–124319.